FRONTIERS OF PHYSICS

RESEARCH ARTICLE
Volume 22 / Issue 4 / 045201 / 2027

All-electrically controlled topological Josephson diode in quantum anomalous Hall insulator–superconductor hybrids

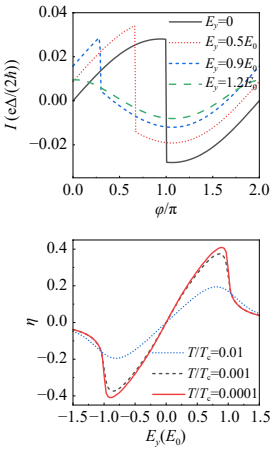
Kang-Ze Li[1], Yong Xu[2], Jun Wang[3,†], Pei-Hao Fu[1,‡], Jun-Feng Liu[1,§]

1 School of Physics and Materials Science, Guangzhou University, Guangzhou 510006, China
2 Institute of Materials, Ningbo University of Technology, Ningbo 315016, China
3 Department of Physics, Southeast University, Nanjing 210096, China
Corresponding authors. E-mail: †jwang@seu.edu.cn, ‡phy.phfu@gmail.com, §phjfliu@gzhu.edu.cn
Received July 5, 2026; accepted September 24, 2026

© Higher Education Press 2027

ABSTRACT

We propose and investigate an all-electrically controlled Josephson diode effect in a hybrid junction consisting of a quantum anomalous Hall insulator (QAHI) sandwiched between two topological superconductors (TSCs). Due to the spatial separation of two paired electrons from the chiral edge states, a transverse electric field applied across the two TSC leads imposes different energies on two paired electrons and modifies the spectrum of chiral Andreev bound states, consequently generating a sizable nonreciprocal supercurrent without the need for external magnetic fields. We further demonstrate two additional electrical control mechanisms: (i) tuning the chemical potential enhances the diode response by separating the superconducting gap from finite-size-induced gaps; and (ii) applying asymmetric electric fields to the two TSC leads enables precise and continuous modulation of the diode efficiency while preserving its polarity. The induced diode effect is shown to be robust against moderate disorders. Our results establish electrostatic gating as a powerful and practical approach to engineer and control nonreciprocal superconducting transport, providing a general framework for realizing electrically tunable topological Josephson diodes.



Keywords quantum anomalous Hall insulator, topological superconductor, Josephson diode

1 Introduction

Josephson diodes, which exhibit a nonreciprocal supercurrent, have garnered significant interest for their potential applications in superconducting electronics and quantum information technologies [1–15]. The ability to generate a directional supercurrent is a key functionality for developing next-generation superconducting circuits and quantum architectures [16–27].

It is well established that the superconducting diode effect requires the simultaneous breaking of both inversion symmetry and time-reversal symmetry (TRS) [28–30]. Once these symmetries are lifted, a unidirectional component emerges in the supercurrent, leading to nonreciprocal transport. Microscopically, the nonreciprocity can originate from finite-momentum Cooper pairing [6, 31–34], vortex-related phenomena [35], or spatial asymmetry due to phase-interference patterns [7]. Inversion-symmetry breaking typically relies on careful geometric design, making the diode efficiency highly sensitive to structural parameters [36] and difficult to tune after fabrication. Consequently, most experimental

https://doi.org/10.15302/frontphys.2027.045201

demonstrations rely on external magnetic fields to break TRS and activate or modulate the diode response.

However, strong magnetic fields inevitably suppress superconductivity, posing a fundamental limitation [37]. This has motivated the search for magnetic-field-free superconducting diodes [38–52], where TRS is broken intrinsically via magnetic order. Nevertheless, even in these systems, external magnetic fields are often still required for polarity switching or on/off control [43]. Therefore, a fully electrical scheme for generating and tuning the diode effect, entirely without magnetic fields, remains highly desirable for scalable superconducting circuitry.

On the other hand, realizing the Josephson diode effect in topological systems could lead to a topological Josephson diode [10–13], where the supercurrent is carried by topologically protected edge states, such as helical states in quantum spin Hall insulators [53–55] or Majorana bound states in topological superconductors [56–59], often supported by strong spin-orbit coupling [60, 61]. Despite their topological robustness, most proposed platforms still rely on magnetic-field-induced asymmetry to achieve the diode effect [14, 15, 44, 61, 62]. Moreover, practical implementations typically require complex magnetic-field configurations or additional control parameters [63–66], making the realization of a robust and tunable topological Josephson diode experimentally challenging [65–70]. While Josephson junctions based on quantum spin Hall insulators and topological superconductors have been extensively studied [53–59, 71], those based on quantum anomalous Hall insulators (QAHIs) [72–76] remain relatively rare.

In this work, we propose an all-electrical scheme to realize and control a topological Josephson diode in a QAHI-superconductor hybrid junction, where the diode efficiency is tuned solely by transverse electric fields and the chemical potential. We consider a junction composed of a QAHI coupled to two topological superconductors (TSCs), as sketched in Fig. 1. We first demonstrate that a transverse electric field induces a pronounced band asymmetry in the chiral edge states of the QAHI, effectively mimicking the role of finite-momentum Cooper pairing

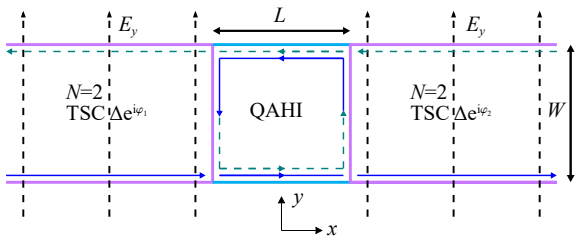


Fig. 1 A Josephson junction composed of a quantum anomalous Hall insulator (QAHI) sandwiched between two $N = 2$ TSCs. Blue (green) solid (dashed) arrows represent the transport modes of electrons (holes). Nonlocal ABSs emerge in the central QAHI region. A transverse electric field E_y is applied in the TSC regions, increasing the potential energy linearly from the bottom to the top boundary.

induced by magnetic fields (Fig. 2). This electrically induced asymmetry produces an anomalous Josephson effect and a significant diode efficiency (Fig. 3), manifested in the asymmetric Andreev bound state (ABS) spectrum (Fig. 4). We then systematically examine the influence of chemical potential, device geometry, temperature, and disorder, demonstrating the robustness and high tunability of the proposed approach (Figs. 5–7). Our findings provide a realistic route toward magnetic-field-free, electrically tunable Josephson diodes and establish a theoretical framework for optimizing diode performance in QAHI-based hybrid devices.

The remainder of the paper is organized as follows. Section 2 introduces the theoretical model and formalism for the TSC-QAHI-TSC Josephson junction. Section 3 presents the main results and discussion. Conclusions are given in Section 4.

2 Model and formalism

We consider a narrow QAHI ribbon in which the wave functions of edge states from opposite boundaries overlap. When the Fermi energy lies within the topological bulk gap, the proximity effect of an s-wave superconductor induces a transition from the QAHI into a TSC with

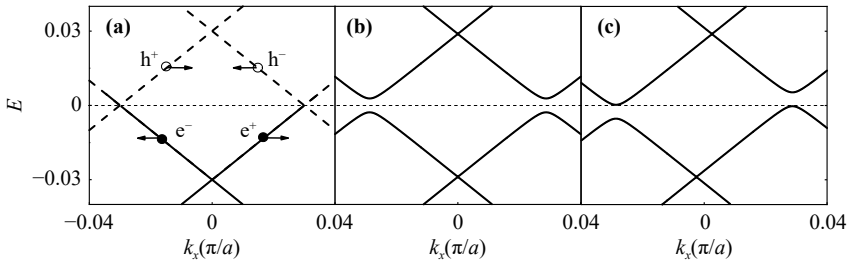


Fig. 2 Energy spectra of electronlike and holelike edge states in the QAHI or the $N = 2$ TSC ribbon with width $W = 11$. Solid (hollow) circles represent electronlike (holelike) states. Plus (minus) signs denote spin-up (spin-down) states. Arrows indicate the propagation direction. **(a)** Both superconducting pairing and the transverse electric field are absent, i.e., $\Delta = 0$ and $E_y = 0$. **(b)** $\Delta = 0.1$ and $E_y = 0$. **(c)** $\Delta = 0.1$ and $E_y = E_0$ with E_0 being a critical transverse electric field.

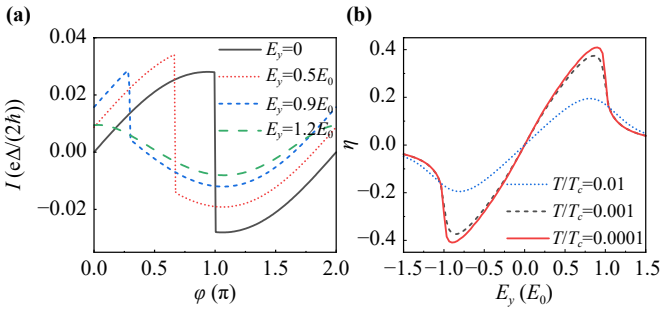


Fig. 3 **(a)** Current-phase relations (CPR) under different transverse electric fields E_y, ranging from 0 to $1.2E_0$. An increasing E_y induces both an anomalous phase shift and pronounced asymmetry. **(b)** Diode efficiency η as a function of the transverse electric field E_y at different temperatures. A maximum efficiency $\eta \simeq 41\%$ is achieved at $E_y = 0.9E_0$. The system parameters are: $A = B = 1$, $m = 0.5$, $\mu_N = 0$, $\mu_s = 0.03$, $\Delta = 0.1$, $W = 11a$, $L = 2a$, and $E_0 = 0.0035$.

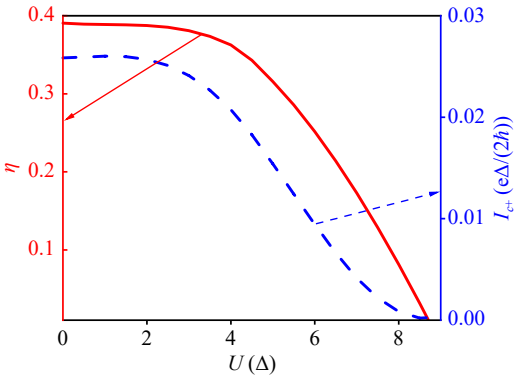


Fig. 5 Diode efficiency η (red curve) and forward critical current I_{c+} (blue curve) as functions of the disorder strength U. The QAHI region length is $L = 10a$. The diode effect remains robust for moderate disorder ($U < 4\Delta$) but is rapidly suppressed for stronger disorder.

Chern number $N = 2$. We investigate the Josephson diode effect in junctions consisting of a QAHI with length L sandwiched between two such TSCs, as indicated in Fig. 1.

We model the QAHI using the low-energy effective Hamiltonian [77–79]

$$H_{\mathrm{QAHI}} = \left(m - Bk^2\right)\sigma_z + A\left(k_x\sigma_x + k_y\sigma_y\right) \tag{1}$$

in the basis $(c_{\boldsymbol{k}\uparrow}, c_{\boldsymbol{k}\downarrow})^{\mathrm{T}}$, where $c_{\boldsymbol{k}\uparrow(\downarrow)}$ annihilates an electron with momentum $\boldsymbol{k}$ and spin $\uparrow(\downarrow)$. Here $\sigma_{x,y,z}$ are Pauli matrices in spin space, A parameterizes the spin–orbit coupling strength, and m and B are material parameters. The QAHI phase occurs for $m/B > 0$. When the QAHI is proximitized by an s-wave superconductor, a pairing potential Δ is induced and the resulting Bogoliubov–de Gennes (BdG) Hamiltonian becomes [77]

$$H_{\mathrm{BdG}} = \begin{pmatrix} H_{\mathrm{QAHI}}(\boldsymbol{k}) - \mu_S & \mathrm{i}\Delta\sigma_y \\ -\mathrm{i}\Delta^*\sigma_y & -H^*_{\mathrm{QAHI}}(-\boldsymbol{k}) + \mu_S \end{pmatrix}, \tag{2}$$

written in the Nambu basis $(c_{k\uparrow}, c_{k\downarrow}, c^\dagger_{-k\uparrow}, c^\dagger_{-k\downarrow})^{\mathrm{T}}$. For $m < \sqrt{\Delta^2 + \mu_S^2}$, the system enters a topological superconducting phase with Chern number $N = 2$.

To describe a finite-width ribbon along the y direction, we discretize the Hamiltonian on a square lattice. The lattice BdG Hamiltonian is

$$\begin{aligned} H = &\sum_{\boldsymbol{r}} \Psi^\dagger_{\boldsymbol{r}} \begin{pmatrix} h_0 - \mu & \mathrm{i}\Delta\sigma_y \\ -\mathrm{i}\Delta^*\sigma_y & -h_0^* + \mu \end{pmatrix} \Psi_{\boldsymbol{r}} \\ &+ \sum_{\boldsymbol{r},\boldsymbol{r}_0} \left[\Psi^\dagger_{\boldsymbol{r}} \begin{pmatrix} h_{\boldsymbol{r}_0} & 0 \\ 0 & -h^*_{\boldsymbol{r}_0} \end{pmatrix} \Psi_{\boldsymbol{r}+\boldsymbol{r}_0} + H.c. \right], \end{aligned} \tag{3}$$

where $\boldsymbol{r} = (x, y)$ labels lattice sites, $\boldsymbol{r}_0 = \boldsymbol{x}, \boldsymbol{y}$ denotes the unit vectors along the x and y directions, and $\Psi_{\boldsymbol{r}} = (c_{\boldsymbol{r}\uparrow}, c_{\boldsymbol{r}\downarrow}, c^\dagger_{\boldsymbol{r}\uparrow}, c^\dagger_{\boldsymbol{r}\downarrow})^{\mathrm{T}}$. The on-site and hopping matrices are

$$\begin{aligned} h_0 &= \left(m - \frac{4B\hbar^2}{a^2}\right)\sigma_z, \\ h_{\boldsymbol{x}} &= \frac{B\hbar^2}{a^2}\sigma_z - \frac{\mathrm{i}A}{2}\sigma_x, \\ h_{\boldsymbol{y}} &= \frac{B\hbar^2}{a^2}\sigma_z - \frac{\mathrm{i}A}{2}\sigma_y, \end{aligned} \tag{4}$$

where a is the lattice constant. The chemical potential is set to $\mu = \mu_N$ in the QAHI region and $\mu = \mu_S$ in the superconducting leads.

Moreover, a transverse electric field E_y has also been considered in the leads and modelled by linearly increasing on-site energies along the y direction. It can be equivalently modelled by the modification of the chemical potential

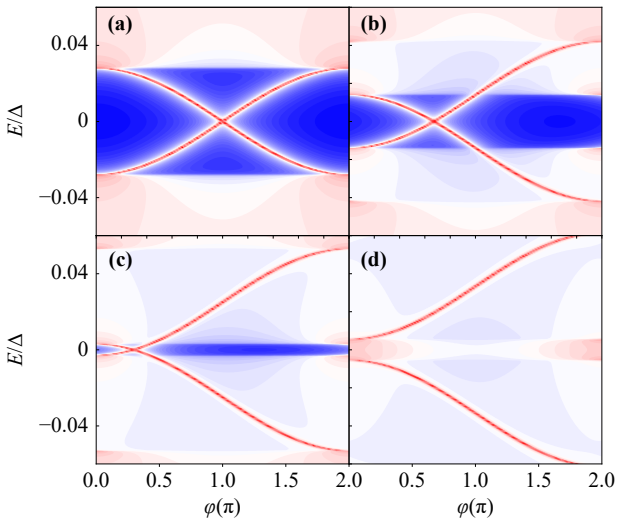


Fig. 4 ABS spectra under different transverse electric fields: **(a)** $E_y = 0$, **(b)** $E_y = 0.5E_0$, **(c)** $E_y = 0.9E_0$, and **(d)** $E_y = 1.2E_0$. Other parameters are consistent with those in Fig. 3(a).

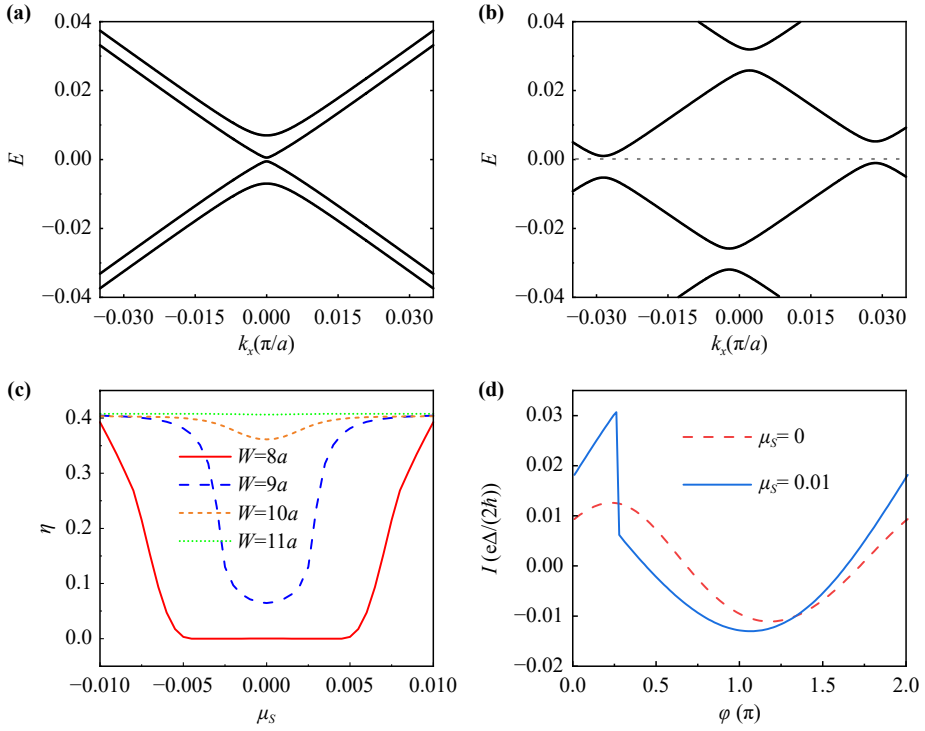


Fig. 6 **(a)** Band structure for a narrow TSC ribbon with $W = 9a$ and $\mu_S = 0$, showing the suppression of the superconducting gap due to finite-size-induced minigaps. **(b)** Band structure at $\mu_S = 0.03$, where the chemical potential separates the superconducting gaps from the finite-size-induced gaps. **(c)** Diode efficiency η as a function of the chemical potential μ_S for different ribbon widths. **(d)** CPR curves for a ribbon of width $W = 9a$ at different chemical potentials.

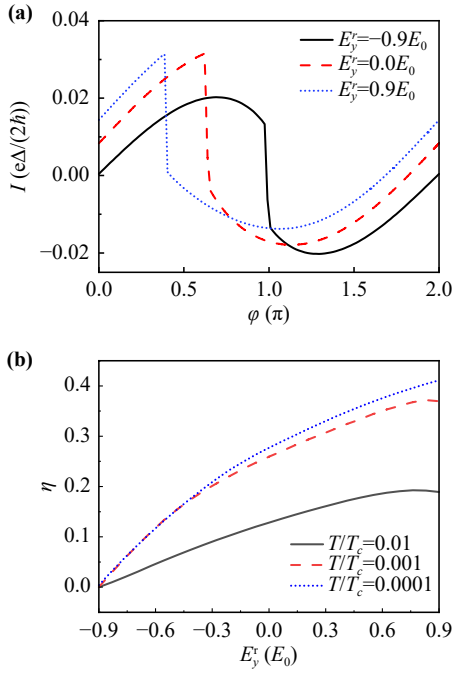


Fig. 7 **(a)** Current-phase relation with a fixed left-side electric field $E_y^l = 0.9E_0$ and varying right-side electric fields E_y^r. **(b)** Diode efficiency η as a function of the right-side electric field E_y^r at different temperatures. The diode polarity is preserved for all E_y^r.

$\mu_S \to \mu_S + eE_y y$ with e the unit charge. We emphasize that E_y is not a macroscopic electric field penetrating the superconductor, but rather an effective description of a local electrostatic gating effect. In practice, such a potential gradient can be realized by placing a split gate above the TSC leads, with a voltage difference applied between the two halves of the gate. Alternatively, one can use a side gate or a dielectric layer with a built-in field gradient. The proximity-induced superconductivity in the QAHI is governed by the interface, the gating effectively modifies the chemical potential of the surface states that participate in the Andreev processes. Our model captures this effect by a position-dependent chemical potential in the leads.

The Josephson current flowing through column l of the QAHI region is computed using the nonequilibrium Green's function formalism:

$$I = \frac{1}{h}\int_{-\infty}^{\infty} \mathrm{Tr}\left[\check{t}^{\dagger}\check{e}\,G^{<}_{l,l-1} - \check{e}\check{t}\,G^{<}_{l-1,l}\right]\mathrm{d}E, \tag{5}$$

where

$$\check{t} = \frac{B\hbar^2}{a^2}\,\tau_z\otimes\sigma_z + \frac{\mathrm{i}A}{2}\,\tau_0\otimes\sigma_x, \quad \check{e} = -e\,\tau_z\otimes\sigma_0. \tag{6}$$

Here $\tau_{0,z}$ are Pauli matrices in Nambu space. In equilibrium, $G^{<} = f(E)(G^a - G^r)$, with $f(E)$ being the Fermi–

Dirac function. The retarded/advanced Green functions are given by

$$G^r(E) = \frac{1}{E - H_N - \Sigma_L^r(E) - \Sigma_R^r(E)}, \quad G^a = (G^r)^\dagger, \tag{7}$$

where H_N is the Hamiltonian of the QAHI region, and $\Sigma_{L,R}^r$ denote the self-energies of the left and right superconducting leads, evaluated using a recursive method [80, 81].

To characterize the diode effect, the degree of nonreciprocity, i.e., the diode efficiency in the Josephson junction, is quantified as

$$\eta = \frac{I_{c+} - I_{c-}}{I_{c+} + I_{c-}}, \tag{8}$$

where I_{c+} and I_{c-} denote the forward and reverse critical currents, respectively [28, 32, 35, 82–84]. The forward and backward critical currents are extracted numerically from the current-phase relation. This measure captures the directional asymmetry of the supercurrent and characterizes the strength of the diode effect [33, 85].

The ABS spectrum is obtained from the local density of states (LDOSs),

$$\rho_l(E) = -\frac{1}{\pi} \mathrm{Im}\{\mathrm{Tr}[G^r(l,l;E)]\}, \tag{9}$$

computed for column l at a fixed phase difference $\phi = \phi_L - \phi_R$. The peaks of LDOSs inside the superconducting gap locate the ABS energy levels.

The above model establishes a unified framework for describing TSC-QAHI-TSC Josephson junctions and evaluating their transport properties under external electric fields and variable chemical potential. Unless otherwise specified, we adopt the following parameters throughout this work: $A = B = 1$, $m = 0.5$, $\mu_N = 0$, $\mu_S = 0.03$, $\Delta = 0.1$, $W = 11a$, $E_0 = 0.0007$, and $L = 2a$. In general, the critical electric field satisfies $E_0(W-1)/2 \approx \Delta'$ with Δ' the real superconducting gap. Due to the finite penetration depth of QAH edge states, the effect of the electric field is slightly weakened. It means that E_0 should be slightly larger than the expected value.

3 Results and discussion

3.1 Transverse electric field controlled topological Josephson diode

We now present an analysis of the electrically tunable Josephson diode effect in the TSC–QAHI–TSC junction shown in Fig. 1. First, we investigate the band spectra of the central QAHI ribbon and two TSC lead ribbons by assuming that all three parts are infinite along the x direction. The band spectra are obtained numerically by diagonalizing the lattice Hamiltonian described by Eqs. (3) and (4) for a ribbon geometry. Figure 2 schematically illustrates the energy spectra of chiral electronlike and holelike edge states in the QAHI or the $N = 2$ TSC leads. In the chiral edge states of QAHI, the right-moving (left-moving) electrons locate at the bottom (top) edge. By proximitizing with an s-wave superconductor, the electron and the hole at opposite edges couple each other due to the narrow size of the ribbon, resulting in a superconducting gap $\Delta' < \Delta$ shown in Fig. 2(b). A right-moving (left-moving) electron couples with a left-moving (right-moving) hole to form a superconducting gap at positive (negative) Fermi momentum k_F. Due to the nonlocal nature of the Cooper pairs, a transverse electric field E_y endows two paired electrons with different potential energies. Since the hole has the opposite energy of the electron, the gap located at positive (negative) k_F moves upwards (downwards) in the energy spectra as shown in Fig. 2(c) where a critical $E_y = E_0$ is applied. In the energy region $[-2\Delta', 0]$, a right-moving electron in the central QAHI will be transmitted as an electronlike wave in the right TSC, while a left-moving electron will be reflected into a hole. Similarly, a left-moving hole will be transmitted as a holelike wave in the left TSC, while a right-moving hole will be reflected into an electron. Therefore, the left-moving electron and the right-moving hole form an ABS while the right-moving electron and the left-moving hole remain continuum states in the central QAHI. These ABSs [86–89] are inherently chiral and nonlocal, with electrons and holes spatially separated along opposite edges of the QAHI. The nonlocal nature of these ABSs underlies the electric-field tunability of the supercurrent nonreciprocity. As indicated in the energy region $[-2\Delta', 0]$ of Fig. 2(c), the forward supercurrent is dominated by continuum states, whereas the backward supercurrent arises primarily from ABS. Since the contribution from continuum states exceeds that from the ABS, a positive diode efficiency results, consistent with the data shown in Fig. 3(a).

As discussed above, the field-induced asymmetry between the two superconducting gaps at $\pm k_F$ results in an imbalance between the forward and backward supercurrents, leading to a Josephson diode effect. From the symmetry point of view, the Hamiltonian in Eq. (1) has a symmetry related to $R_x R_y \sigma_z$ which prohibits the Josephson diode effect. When a transverse electric field is applied, this symmetry is broken and hence the diode effect occurs. As E_y increases toward a critical value E_0, the asymmetry becomes substantial. Figure 3(a) shows the current-phase relation (CPR) under varying electric field at a low temperature ($T/T_c = 10^{-4}$). At $E_y = 0$, the CPR exhibits a distorted sinusoidal shape with no Josephson diode effect. Increasing E_y induces both an anomalous phase shift and a clear asymmetry between the forward and backward supercurrent.

The critical currents are defined as $I_{c+} = \max_\phi I(\phi)$ and $I_{c-} = |\min_\phi I(\phi)|$. Figure 3(b) presents the resulting diode efficiency η as a function of E_y for different temperatures. The diode efficiency is antisymmetric with respect to the electric field. A maximum efficiency of $\eta \simeq 41\%$ is achieved at $E_y = 0.9E_0$, comparable to values reported for magnetically controlled junctions. For $E_y > 0.9E_0$, η decreases rapidly due to the suppression of the Josephson current [see Fig. 3(a)].

The numerically computed ABS spectra are presented in Fig. 4. When $E_y = 0$, both the rightward and leftward ABSs (carrying rightward and leftward supercurrents, respectively) occur in the energy region $[-\Delta', \Delta]$, the continuum states carry no supercurrent. Under the transverse electric field E_y, as shown in Fig. 4(b), the two ABSs experience opposite energy shifts: the rightward ABS is pushed upward while the leftward ABS is pulled downward. This behavior mirrors exactly the field-induced asymmetry of the superconducting gaps at $\pm k_F$ displayed in Fig. 2. Because the two ABSs carry currents in opposite directions near the Fermi level, their asymmetric energy shifts break the symmetry between the forward and backward current contributions. Consequently, the total supercurrent becomes nonreciprocal. When $E_y = 0.9E_0$, the leftward ABS shifts to nearly $[-2\Delta', 0]$ while the rightward ABS shifts almost above the Fermi energy. Now the rightward supercurrent is mainly carried by the continuum states in the energy region $[-2\Delta', 0]$. The evolution of two ABSs clarifies the origin of the key features observed in the CPRs of Fig. 3(a): both the increasing phase shift and the enhancement of the diode efficiency with rising E_y stem from these opposite energy shifts of the two ABSs. This direct correspondence between the ABS evolution and the CPR features establishes a clear microscopic picture: the electrically controlled ABS imbalance is the root cause of the Josephson diode effect in our system.

3.2 Robustness of electrically tunable topological Josephson diodes

Having established the electrically induced Josephson diode effect in QAHI–TSC junctions, we now examine its robustness against realistic perturbations. While topological edge states generally provide strong protection against backscattering, device-specific factors such as disorder, finite-size hybridization, and asymmetric gating may modify the ABS structure and thus the diode response. In this section, we analyze the influence of disorder, sample width, chemical potential, and asymmetric electric fields, demonstrating that the electrically controlled diode effect remains robust, highly tunable and resilient over a broad parameter regime.

3.2.1 Effect of disorder

The chiral nature of the QAHI edge states ensures that the Josephson current is robust against moderate disorder. To quantify this robustness, we extend the QAHI length to $L = 10a$ and introduce on-site disorder with random potentials uniformly distributed in the range $[-U, U]$. As shown in Fig. 5, for $U < 4\Delta$, the diode efficiency η and forward critical current I_{c+} exhibit only minor reductions, indicating that the topological edge channels remain well protected. However, when $U > 4\Delta$, strong disorder begins to enhance the coupling between two edge modes, leading to a rapid suppression of both η and I_{c+}. At sufficiently large disorder strengths, the diode effect vanishes entirely, signaling the breakdown of coherent topological transport.

3.2.2 Finite-size effect and chemical-potential control

In addition to disorder, finite-size effects can influence the Josephson diode response. For narrow ribbons where the width W approaches the localization length of the edge states, the finite-size coupling between two electron states on opposite boundaries opens a finite-size-induced minigap [90]. In TSCs, the superconducting gap induced by the proximity effect also originates from the finite-size coupling between electron and hole states on opposite boundaries, resulting in a gap magnitude comparable to that of the finite-size gap. Unlike the superconducting gap, however, the finite-size gap oscillates with the width. Figures 6(a) and (b) present the energy spectrum for $W = 9a$. In Fig. 6(b), the two superconducting gaps are located at $k_x = \pm k_F$, while the two finite-size gaps appear near $k_x = 0$. Compared with the spectrum for $W = 11a$ in Fig. 2(c), the finite-size gaps here become negligibly small, whereas the superconducting gaps remain nearly unchanged in magnitude. When the chemical potential approaches zero, the Fermi wave vector vanishes ($k_F = 0$), causing the superconducting gap and the finite-size gap to overlap. Their interplay strongly modifies the superconducting gap, making it extremely small, as shown in Fig. 6(a).

Therefore, the interplay between the superconducting gap and the finite-size gap underlies the chemical potential modulation of both the critical Josephson current and the diode efficiency. Figure 6(c) plots the diode efficiency η as a function of the chemical potential μ_s for different ribbon widths. For the ribbon with $W = 11a$, the diode efficiency is independent of the chemical potential, while for the ribbon with other widths, the diode efficiency is significantly modulated by the chemical potential μ_s. Figure 6(d) plots the CPRs for a ribbon of width $W = 9a$ at different chemical potentials. It is seen that the critical currents are also heavily modulated by μ_s due to the change in the superconducting gap.

3.2.3 Asymmetric electric-field modulation

Besides global chemical potential tuning, the Josephson

diode can be further tailored using asymmetric electric fields applied independently to the left and right TSC leads. We denote the transverse fields as E_y^l and E_y^r for the left and right TSC leads, respectively. Fixing the left-lead field at $E_y^l = 0.9E_0$ and sweeping E_y^r allows us to unbalance the spectra in the two leads.

As shown in Fig. 7(a), varying E_y^r modifies the phase shift and the imbalance between the positive and negative critical current of the CPR. When $E_y^r = -0.9E_0$, the energy shifts of the two superconducting gaps in the spectrum of the right TSC are opposite to those for the left TSC shown in Fig. 2(c). In this antisymmetric field configuration, the diode effect vanishes. For $E_y^r = 0.9E_0$, the diode efficiency recovers its maximum 41%. The case $E_y^r = 0$ corresponds to the intermediate situation between these two extremes. As illustrated in Fig. 7(b), the diode efficiency can be continuously adjusted from zero to its maximum value solely by E_y^r. Importantly,the diode polarity remains unchanged for all E_y^r, in contrast to the polarity reversal observed under symmetric electric-field tuning. Such one-sided modulation provides a distinct device-level advantage: it simplifies control while enabling precise and monotonic tuning of the diode efficiency.

4 Conclusion

We have demonstrated an electrically tunable topological Josephson diode based on a TSC-QAHI-TSC junction. It is shown that a transverse electric field can efficiently induce antisymmetric shifts of two superconducting gaps (relevant to forward and backward supercurrents, respectively), modify the ABS dispersion, and generate a sizable diode efficiency (up to $\sim 41\%$) without relying on magnetic fields. Besides global electric gating, we introduced two additional electrical control strategies. First, tuning the chemical potential effectively modulates the diode efficiency and the supercurrent magnitude for some ribbon widths by tuning the overlap between the superconducting gap and the finite-size-induced minigaps. Second, applying asymmetric electric fields to the left and right TSC leads enables precise, polarity-preserving control of the diode efficiency. We further demonstrated that the electrically induced diode effect is robust against moderate disorders. Overall, our results establish electrostatic gating as a versatile and robust tool for engineering nonreciprocal superconducting transport in topological systems. This work provides a platform for designing all-electrically controlled Josephson diodes.

Declarations The authors declare that they have no competing interests and there are no conflicts.

Data availability The data supporting the findings of this study are available from the corresponding authors upon reasonable request.

Author contributions K.-Z. L. developed the theoretical model, performed calculations, and wrote the manuscript. J.-F. L., P.-H. F., and J. W. supervised the project. Y. X. provided valuable insights and contributed to the analysis and interpretation of the results. All authors discussed the results and contributed to the final version of the manuscript.

Acknowledegments The work described in this paper was supported by the National Natural Science Foundation of China (Grant Nos. 12174077 and 12174051).

References

1. J. Wang, Y. Jiang, J. J. Wang, and J. F. Liu, Efficient Josephson diode effect on a two-dimensional topological insulator with asymmetric magnetization, *Phys. Rev. B* 109(7), 075412 (2024)
2. J. J. He, Y. Tanaka, and N. Nagaosa, A phenomenological theory of superconductor diodes, *New J. Phys.* 24(5), 053014 (2022)
3. Y. Zhang, Y. Gu, P. Li, J. Hu, and K. Jiang, General theory of Josephson diodes, *Phys. Rev. X* 12(4), 041013 (2022)
4. M. Nadeem, M. S. Fuhrer, and X. Wang, The superconducting diode effect, *Nat. Rev. Phys.* 5(10), 558 (2023)
5. S. Qi, J. Ge, C. Ji, Y. Ai, G. Ma, Z. Wang, Z. Cui, Y. Liu, Z. Wang, and J. Wang, High-temperature field-free superconducting diode effect in high-T_c cuprates, *Nat. Commun.* 16(1), 531 (2025)
6. M. Davydova, S. Prembabu, and L. Fu, Universal Josephson diode effect, *Sci. Adv.* 8(23), eabo0309 (2022)
7. R. S. Souto, M. Leijnse, and C. Schrade, Josephson diode effect in supercurrent interferometers, *Phys. Rev. Lett.* 129(26), 267702 (2022)
8. A. Daido and Y. Yanase, Unidirectional superconductivity and superconducting diode effect induced by dissipation, *Phys. Rev. B* 111(2), L020508 (2025)
9. J. Hu, C. Wu, and X. Dai, Proposed design of a Josephson diode, *Phys. Rev. Lett.* 99(6), 067004 (2007)
10. M. Gupta, G. V. Graziano, M. Pendharkar, J. T. Dong, C. P. Dempsey, C. Palmstrøm, and V. S. Pribiag, Gate-tunable superconducting diode effect in a three-terminal Josephson device, *Nat. Commun.* 14(1), 3078 (2023)
11. B. Pal, A. Chakraborty, P. K. Sivakumar, M. Davydova, A. K. Gopi, A. K. Pandeya, J. A. Krieger, Y. Zhang, M. Date, S. Ju, N. Yuan, N. B. M. Schröter, L. Fu, and S. S. P. Parkin, Josephson diode effect from Cooper pair momentum in a topological semimetal, *Nat. Phys.* 18(10), 1228 (2022)
12. S. Fracassi, S. Traverso, N. Traverso Ziani, M. Carrega, S. Heun, and M. Sassetti, Anomalous supercurrent and diode effect in locally perturbed topological Josephson junctions, *Appl. Phys. Lett.* 124(24), 242601 (2024)
13. B. Lu, S. Ikegaya, P. Burset, Y. Tanaka, and N. Nagaosa, Tunable Josephson diode effect on the surface of topo–logical insulators, *Phys. Rev. Lett.* 131(9), 096001 (2023)
14. Z. Liu, L. Huang, and J. Wang, Josephson diode effect in topological superconductors, *Phys. Rev. B* 110(1),

014519 (2024)
15. J. X. Hu, Z. T. Sun, Y. M. Xie, and K. T. Law, Josephson diode effect induced by valley polarization in twisted bilayer graphene, *Phys. Rev. Lett.* 130(26), 266003 (2023)
16. S. Matsuo, T. Imoto, T. Yokoyama, Y. Sato, T. Lindemann, S. Gronin, G. C. Gardner, M. J. Manfra, and S. Tarucha, Josephson diode effect derived from short-range coherent coupling, *Nat. Phys.* 19(11), 1636 (2023)
17. K. K. Likharev, Dynamics of Josephson Junctions and Circuits, Routledge, 2022, pp 18–22
18. C. Baumgartner, L. Fuchs, A. Costa, S. Reinhardt, S. Gronin, G. C. Gardner, T. Lindemann, M. J. Manfra, P. E. Faria Junior, D. Kochan, J. Fabian, N. Paradiso, and C. Strunk, Supercurrent rectification and magnetochiral effects in symmetric Josephson junctions, *Nat. Nanotechnol.* 17(1), 39 (2022)
19. I. V. Bobkova, A. M. Bobkov, and M. A. Silaev, Magnetoelectric effects in Josephson junctions, *J. Phys.: Condens. Matter* 34(35), 353001 (2022)
20. R. Seoane Souto, M. Leijnse, C. Schrade, M. Valentini, G. Katsaros, and J. Danon, Tuning the Josephson diode response with an ac current, *Phys. Rev. Res.* 6(2), L022002 (2024)
21. S. Reinhardt, T. Ascherl, A. Costa, J. Berger, S. Gronin, G. C. Gardner, T. Lindemann, M. J. Manfra, J. Fabian, D. Kochan, C. Strunk, and N. Paradiso, Link between supercurrent diode and anomalous Josephson effect revealed by gate-controlled interferometry, *Nat. Commun.* 15(1), 4413 (2024)
22. M. Coraiola, A. E. Svetogorov, D. Z. Haxell, D. Sabonis, M. Hinderling, S. C. ten Kate, E. Cheah, F. Krizek, R. Schott, W. Wegscheider, J. C. Cuevas, W. Belzig, and F. Nichele, Flux-tunable Josephson diode effect in a hybrid four-terminal Josephson junction, *ACS Nano* 18(12), 9221 (2024)
23. S. Chen, S. Park, U. Vool, N. Maksimovic, D. A. Broadway, M. Flaks, T. X. Zhou, P. Maletinsky, A. Stern, B. I. Halperin, and A. Yacoby, Current induced hidden states in Josephson junctions, *Nat. Commun.* 15(1), 8059 (2024)
24. J. F. Steiner, L. Melischek, M. Trahms, K. J. Franke, and F. von Oppen, Diode effects in current-biased Josephson junctions, *Phys. Rev. Lett.* 130(17), 177002 (2023)
25. A. Banerjee, O. Lesser, M. A. Rahman, H. R. Wang, M. R. Li, A. Kringhøj, A. M. Whiticar, A. C. C. Drachmann, C. Thomas, T. Wang, M. J. Manfra, E. Berg, Y. Oreg, A. Stern, and C. M. Marcus, Signatures of a topological phase transition in a planar Josephson junction, *Phys. Rev. B* 107(24), 245304 (2023)
26. R. Mélin, C. B. Winkelmann, and R. Danneau, Magnetointerferometry of multiterminal Josephson junctions, *Phys. Rev. B* 109(12), 125406 (2024)
27. D. C. Ohnmacht, M. Coraiola, J. J. García-Esteban, D. Sabonis, F. Nichele, W. Belzig, and J. C. Cuevas, Quartet tomography in multiterminal Josephson junctions, *Phys. Rev. B* 109(24), L241407 (2024)
28. B. Zinkl, K. Hamamoto, and M. Sigrist, Symmetry conditions for the superconducting diode effect in chiral superconductors, *Phys. Rev. Res.* 4(3), 033167 (2022)
29. J. Hu, C. Wu, and X. Dai, Proposed design of a Josephson diode, *Phys. Rev. Lett.* 99(6), 067004 (2007)
30. D. Wang, Q. H. Wang, and C. Wu, Symmetry constraints on direct-current Josephson diodes, arXiv: 2209.12646 (2022)
31. S. Hart, H. Ren, M. Kosowsky, G. Ben-Shach, P. Leubner, C. Brüne, H. Buhmann, L. W. Molenkamp, B. I. Halperin, and A. Yacoby, Controlled finite momentum pairing and spatially varying order parameter in proximitized HgTe quantum wells, *Nat. Phys.* 13(1), 87 (2017)
32. N. F. Q. Yuan and L. Fu, Supercurrent diode effect and finite-momentum superconductors, *Proc. Natl. Acad. Sci. USA* 119(15), e2119548119 (2022)
33. N. F. Q. Yuan and L. Fu, Topological metals and finite-momentum superconductors, *Proc. Natl. Acad. Sci. USA* 118(3), e2019063118 (2021)
34. P. H. Fu, Y. Xu, J. F. Liu, C. H. Lee, and Y. S. Ang, Implementation of a transverse Cooper-pair rectifier using an NS junction, *Phys. Rev. B* 111(2), L020507 (2025)
35. P. Ding, C. H. Lee, X. Wu, and R. Thomale, Diagnosis of pairing symmetry by vortex and edge spectra in kagome superconductors, *Phys. Rev. B* 105(17), 174518 (2022)
36. H. Narita, J. Ishizuka, R. Kawarazaki, D. Kan, Y. Shiota, T. Moriyama, Y. Shimakawa, A. V. Ognev, A. S. Samardak, Y. Yanase, and T. Ono, Field-free superconducting diode effect in noncentrosymmetric superconductor/ferromagnet multilayers, *Nat. Nanotechnol.* 17(8), 823 (2022)
37. R. S. Muller, T. I. Kamins, and M. Chan, Device Electronics for Integrated Circuits, 3rd Ed. John Wiley & Sons, Inc, 2003
38. H. X. Lou, J. J. Chen, X. G. Ye, Z. B. Tan, A. Q. Wang, Q. Yin, L. Xin, J. Z. Fang, X. Y. Liu, Y. L. He, Z. T. Zhang, C. Li, Z. M. Wei, X. M. Ma, D. P. Yu, and Z. M. Liao, Quantized radio-frequency rectification in a kagome superconductor Josephson diode, *Nat. Nanotechnol.* 21(4), 554 (2026)
39. J. X. Lin, P. Siriviboon, H. D. Scammell, S. Liu, D. Rhodes, K. Watanabe, T. Taniguchi, J. Hone, M. S. Scheurer, and J. I. A. Li, Zero-field superconducting diode effect in small-twist-angle trilayer graphene, *Nat. Phys.* 18(10), 1221 (2022)
40. J. Jiang, M. V. Milošević, Y. L. Wang, Z. L. Xiao, F. M. Peeters, and Q. H. Chen, Field-Free Superconducting Diode in a Magnetically Nanostructured Superconductor, *Phys. Rev. Appl.* 18(3), 034064 (2022)
41. T. Golod, and V. M. Krasnov, Demonstration of a superconducting diode-with-memory, operational at zero magnetic field with switchable nonreciprocity, *Nat. Commun.* 13(1), 3658 (2022)
42. F. Zhang, M. T. Ahari, A. S. Rashid, and others, Reconfigurable magnetic-field-free superconducting diode effect in multi-terminal Josephson junctions, arXiv: 2301.05081 (2023)
43. K. R. Jeon, J. K. Kim, J. Yoon, J. C. Jeon, H. Han, A. Cottet, T. Kontos, and S. S. P. Parkin, Zero-field polarity-reversible Josephson supercurrent diodes enabled by a proximity- magnetized pt barrier, *Nat. Mater.* 21(9),

1008 (2022)
44. H. Wu, Y. Wang, Y. Xu, P. K. Sivakumar, C. Pasco, U. Filippozzi, S. S. P. Parkin, Y. J. Zeng, T. McQueen, and M. N. Ali, The field-free Josephson diode in a van der Waals heterostructure, *Nature* 604(7907), 653 (2022)
45. G. P. Mazur, N. van Loo, D. van Driel, J. Y. Wang, G. Badawy, S. Gazibegovic, E. P. A. M. Bakkers, and L. P. Kouwenhoven, Gate-tunable Josephson diode, *Phys. Rev. Appl.* 22(5), 054034 (2024)
46. H. Y. Xie, M. G. Vavilov, and A. Levchenko, Weyl nodes in Andreev spectra of multiterminal Josephson junctions: Chern numbers, conductances, and supercurrent, *Phys. Rev. B* 97(3), 035443 (2018)
47. E. W. Hodt and J. Linder, On-off switch and sign change for a nonlocal Josephson diode in spin-valve Andreev molecules, *Phys. Rev. B* 108(17), 174502 (2023)
48. P. Kotetes, M. Roig, and B. M. Andersen, Nonreciprocal equilibrium Josephson effect of arbitrary periodicity from poor man's Majorana zero modes, *Phys. Rev. B* 113(24), L241403 (2026)
49. J. D. Pillet, S. Annabi, A. Peugeot, H. Riechert, E. Arrighi, J. Griesmar, and L. Bretheau, Joseph-son diode effect in Andreev molecules, *Phys. Rev. Res.* 5(3), 033199 (2023)
50. S. Mondal and J. Cayao, Spin-polarized Andreev molecules and anomalous nonlocal Josephson effects in altermagnetic junctions, *Phys. Rev. Res.* 8(3), 033223 (2026)
51. J. Cayao and M. Sato, Nonlocal Josephson diode effect in minimal Kitaev chains, *Phys. Rev. Res.* 8(1), 013326 (2026)
52. J. H. Correa and M. P. Nowak, Theory of universal diode effect in three-terminal Josephson junctions, *SciPost Phys.* 17, 037 (2024)
53. P. H. Fu, Y. Xu, S. A. Yang, C. H. Lee, Y. S. Ang, and J. F. Liu, Field-effect Josephson diode via asymmetric spin-momentum locking states, *Phys. Rev. Appl.* 21(5), 054057 (2024)
54. H. Huang, T. de Picoli, and J. I. Väyrynen, Superconducting diode effect in two-dimensional topological insulator edges and Josephson junctions, *Appl. Phys. Lett.* 125(3), 032602 (2024)
55. B. Scharf, D. Kochan, and A. Matos-Abiague, Superconducting diode effect in quantum spin Hall insulator based Josephson junctions, *Phys. Rev. B* 110(13), 134511 (2024)
56. H. F. Legg, K. Laubscher, D. Loss, and J. Klinovaja, Parity-protected superconducting diode effect in topological Josephson junctions, *Phys. Rev. B* 108(21), 214520 (2023)
57. J. Cayao, N. Nagaosa, and Y. Tanaka, Enhancing the Josephson diode effect with Majorana bound states, *Phys. Rev. B* 109(8), L081405 (2024)
58. S. Mondal, P. H. Fu, and J. Cayao, Josephson diode effect with Andreev and Majorana bound states, *Phys. Rev. B* 112(14), 144506 (2025)
59. N. Lotfizadeh, W. F. Schiela, B. Pekerten, P. Yu, B. H. Elfeky, W. M. Strickland, A. Matos-Abiague, and J. Shabani, Superconducting diode effect sign change in epitaxial Al-InAs Josephson junctions, *Commun. Phys.* 7(1), 120 (2024)
60. C. Baumgartner, L. Fuchs, A. Costa, J. Picó-Cortés, S. Reinhardt, S. Gronin, G. C. Gardner, T. Lindemann, M. J. Manfra, P. E. Faria Junior, D. Kochan, J. Fabian, N. Paradiso, and C. Strunk, Effect of Rashba and Dresselhaus spin–orbit coupling on supercurrent rectification and magnetochiral anisotropy of ballistic Josephson junctions, *J. Phys.: Condens. Matter* 34(15), 154005 (2022)
61. A. Costa, J. Fabian, and D. Kochan, Microscopic study of the Josephson supercurrent diode effect in Josephson junctions based on two-dimensional electron gas, *Phys. Rev. B* 108(5), 054522 (2023)
62. Q. Cheng and Q. F. Sun, Josephson diode based on conventional superconductors and a chiral quantum dot, *Phys. Rev. B* 107(18), 184511 (2023)
63. L. V. Pupim and M. S. Scheurer, Adatom engineering magnetic order in superconductors: Applications to altermagnetic superconductivity, *Phys. Rev. Lett.* 134(14), 146001 (2025)
64. Y. J. Wei, J. J. Wang, and J. Wang, Josephson diode effect in a line-centered honeycomb lattice based superconductor junction, *Phys. Rev. B* 108(5), 054521 (2023)
65. J. A. Ouassou, A. Brataas, and J. D. C. Linder, Josephson effect in altermagnets, *Phys. Rev. Lett.* 131(7), 076003 (2023)
66. G. Z. X. Yang, Z. T. Sun, Y. M. Xie, et al, Topological altermagnetic Josephson junctions, arXiv: 2502.20283 (2025)
67. S. Banerjee and M. S. Scheurer, Altermagnetic superconducting diode effect, *Phys. Rev. B* 110(2), 024503 (2024)
68. A. Boruah, S. Acharjee, and P. K. Saikia, Field free Josephson diode effect in Ising superconductor/altermagnet Josephson junction, *Phys. Rev. B* 112, 054505 (2025)
69. Q. Cheng, Y. Mao, and Q. F. Sun, Field-free Josephson diode effect in altermagnet/normal metal/altermagnet junctions, *Phys. Rev. B* 110(1), 014518 (2024)
70. D. Chakraborty, and A. M. Black-Schaffer, Perfect superconducting diode effect in altermagnets, arXiv: 2408.07747 (2024)
71. E. Zhang, Z. T. Sun, Z. Jia, J. Yang, J. Yan, L. Ai, Y. M. Xie, Y. Zhang, X. J. Gao, X. Xu, S. Liu, Q. Ma, C. Hu, X. Kou, J. Zou, N. Ni, K. T. Law, S. Dong, and F. Xiu, Observation of edge supercurrent in topological antiferromagnet MnBi2Te4-based Josephson junctions, *Sci. Adv.* 11(20), eads8730 (2025)
72. C. X. Liu, S. C. Zhang, and X. L. Qi, The quantum anomalous Hall effect: theory and experiment, *Annu. Rev. Condens. Matter Phys.* 7(1), 301 (2016)
73. K. He, Y. Wang, and Q. Xue, Quantum anomalous Hall effect, Topological Insulators: Fundamentals and Perspectives, Wiley-VCH Verlag GmbH & Co. KGaA, 2025, pp 357–376
74. H. Weng, R. Yu, X. Hu, X. Dai, and Z. Fang, Quantum anomalous Hall effect and related topological electronic states, *Adv. Phys.* 64(3), 227 (2015)
75. Z. F. Wang, Z. Liu, and F. Liu, Quantum anomalous Hall effect in 2D organic topological insulators, *Phys.*

Rev. Lett. 110(19), 196801 (2013)
76. Y. Okazaki, T. Oe, M. Kawamura, R. Yoshimi, S. Nakamura, S. Takada, M. Mogi, K. S. Takahashi, A. Tsukazaki, M. Kawasaki, Y. Tokura, and N. H. Kaneko, Quantum anomalous Hall effect with a permanent magnet defines a quantum resistance standard, *Nat. Phys.* 18(1), 25 (2022)
77. Y. Xu, P. H. Fu, L. Chen, J. F. Liu, J. Wang, and H. Xu, Electrically modulated anomalous phase shift in Andreev bound states mediated by chiral Majorana modes, *Phys. Rev. B* 105(7), 075409 (2022)
78. X. L. Qi, Y. S. Wu, and S. C. Zhang, Topological quantization of the spin Hall effect in two- dimensional paramagnetic semiconductors, *Phys. Rev. B* 74(8), 085308 (2006)
79. Z. Lu, T. Han, Y. Yao, Z. Hadjri, J. Yang, J. Seo, L. Shi, S. Ye, K. Watanabe, T. Taniguchi, and L. Ju, Extended quantum anomalous Hall states in graphene/hBN moiré superlattices, *Nature* 637(8048), 1090 (2025)
80. D. H. Lee and J. D. Joannopoulos, Simple scheme for surface-band calculations. I, *Phys. Rev. B* 23(10), 4988 (1981)
81. D. H. Lee and J. D. Joannopoulos, Simple scheme for surface-band calculations. II. The Green's function, *Phys. Rev. B* 23(10), 4997 (1981)
82. K. Yasuda, H. Yasuda, T. Liang, R. Yoshimi, A. Tsukazaki, K. S. Takahashi, N. Nagaosa, M. Kawasaki, and Y. Tokura, Nonreciprocal charge transport at topological insulator/superconductor interface, *Nat. Commun.* 10(1), 2734 (2019)
83. M. Masuko, M. Kawamura, R. Yoshimi, et al., Nonreciprocal charge transport in topological superconductor candidate Bi2Te3/PdTe2 heterostructure, *npj Quantum Mater.* 7, 104 (2022)
84. Y. Hou, F. Nichele, H. Chi, A. Lodesani, Y. Wu, M. F. Ritter, D. Z. Haxell, M. Davydova, S. Ilić, O. Glezakou-Elbert, A. Varambally, F. S. Bergeret, A. Kamra, L. Fu, P. A. Lee, and J. S. Moodera, Ubiquitous superconducting diode effect in superconductor thin films, *Phys. Rev. Lett.* 131(2), 027001 (2023)
85. S. Matsuo, R. S. Deacon, S. Kobayashi, Y. Sato, T. Yokoyama, T. Lindemann, S. Gronin, G. C. Gardner, K. Ishibashi, M. J. Manfra, and S. Tarucha, Shapiro response of superconducting diode effect derived from Andreev molecules, *Phys. Rev. B* 111(9), 094512 (2025)
86. Y. Tanaka, Y. Mizuno, T. Yokoyama, K. Yada, and M. Sato, Anomalous Andreev bound state in noncentrosymmetric superconductors, *Phys. Rev. Lett.* 105(9), 097002 (2010)
87. M. Sato, Y. Tanaka, K. Yada, and T. Yokoyama, Topology of Andreev bound states with flat dispersion, *Phys. Rev. B* 83(22), 224511 (2011)
88. C. Jünger, S. Lehmann, K. A. Dick, C. Thelander, C. Schönenberger, and A. Baumgartner, Intermediate states in Andreev bound state fusion, *Commun. Phys.* 6(1), 190 (2023)
89. C. X. Liu, J. D. Sau, T. D. Stanescu, and S. Das Sarma, Andreev bound states versus Majorana bound states in quantum dot-nanowire-superconductor hybrid structures: Trivial versus topological zero-bias conductance peaks, *Phys. Rev. B* 96(7), 075161 (2017)
90. B. Zhou, H. Z. Lu, R. L. Chu, S. Q. Shen, and Q. Niu, Finite size effects on helical edge states in a quantum spin-Hall system, *Phys. Rev. Lett.* 101(24), 246807 (2008)